A Co-planar Stripline Mach-Zehnder Modulator Enabling 160 GBd PAM-4 on an Indium Phosphide Platform

James Arthur Hillier[1], Qian Hu[2], Haoshuo Chen[2], Arezou Meighan[3], Luc Augustin[4], Michael Wale[1,5], Kevin Williams[1], Weiming Yao[1]

[1]*Eindhoven Hendrik Casimir Institute, Eindhoven University of Technology, Eindhoven, The Netherlands*
[2]*Nokia Bell Labs, 600 Mountain Ave., Murray Hill, NJ 07974, USA*
[3]*Infinera Optics B.V., Herengracht 466, 1017 CA Amsterdam, the Netherlands*
[4]*SMART Photonics, Eindhoven, The Netherlands*
[5]*Department of Electronic and Electrical Engineering, University College London, Torrington Place, London WC1E 7JE, UK*
j.a.hillier@tue.nl

Abstract: Large signal measurements are undertaken on electro-optic Mach-Zehnder modulators using a co-planar-stripline design, realised for the first time on a generic InP platform, demonstrating a 320 Gbit/s line rate with a bit error rate of 1.62×10^{-2}. © 2024 The Author(s)

1. Introduction

The demand for ever-growing transmission capacity continuously drives the development of high-speed Mach-Zehnder modulators (MZMs). Several material platforms are capable of offering such devices, but make concessions in one or more key areas. For instance, lithium niobate- and silicon-based modulators are difficult to be integrated with active components [1], while capacitively loaded modulators on the indium phosphide (InP) platform compromise on device length and footprint [2] and specialised layer stacks may inject incompatibilities with generic foundry processes or alter the functionality of other integrated components. Monolithic integration on an InP platform facilitates high electro-optic (EO) efficiency, afforded by the quantum confined Stark effect (QCSE), while accommodating the integration of both active and passive components on a singular chip, paving the way for high-density integrated photonic circuits [3]. For high performance modulators on InP, co-planar stripline (CPS)-MZMs are designed to situate the signal and ground electrodes in close proximity, overlaying the two deeply etched waveguides [4]. This configuration minimises device footprint compared to conventional co-planar waveguide (CPW) electrodes while reducing microwave loss, matching velocity and impedance, preserving a high bandwidth, and ensuring compatibility with the generic foundry process [5]. Prior measurements of these devices verified -6 dB electric-electric (EE) bandwidth, without an applied reverse bias voltage, of ~45 GHz and ~80 GHz for CPS-MZMs with 2 mm and 1 mm long electrodes, respectively, with an estimated half-wave voltage length product, $V_\pi L$, of 0.9 Vcm [6]. The present work unveils open eye diagrams for on-off keying (OOK) signals up to 160 GBd and a bit error rate (BER) of 1.62 x 10^{-2} for 160 GBd 4-level pulse-amplitude modulation (PAM-4) signal, which is below the BER threshold (1.82×10^{-2}) for 25% overhead hard-decision forward error correction (HD-FEC) [7]. To the best of our knowledge, these performance metrics represent the present state of the art for non-coherent InP-based MZMs.

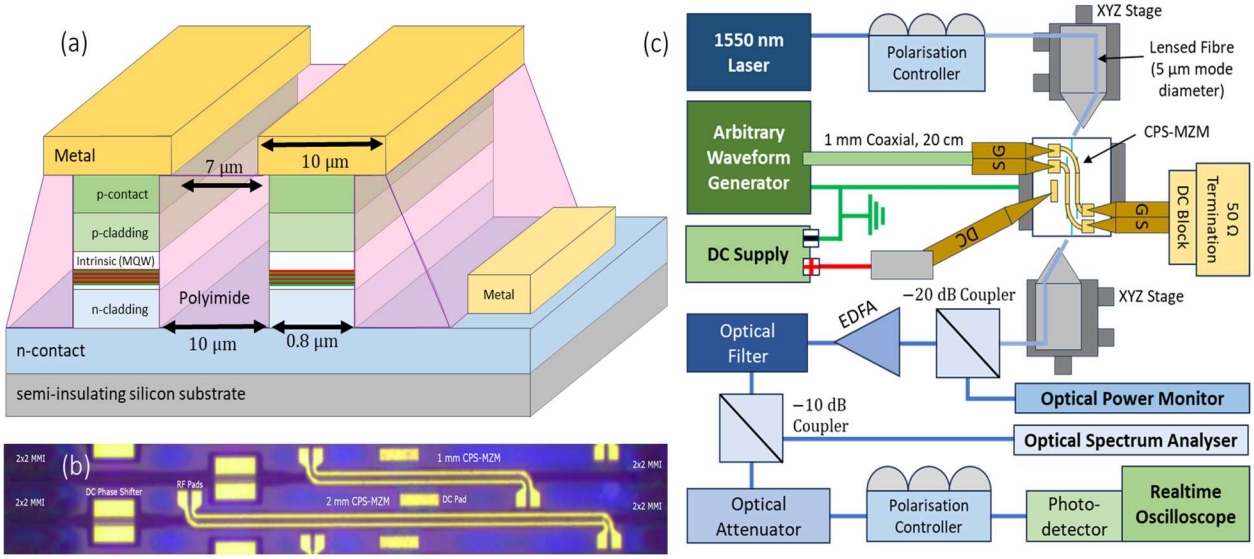

Fig. 1. (a) Schematic illustration of the CPS-MZM on a generic InP platform. (b) Microscope image of a 1 mm and 2 mm CPS-MZM. (c) Schematic of the experimental setup.

1. Device Structure

An array of CPS-MZMs were fabricated on a dedicated wafer run designed using the process design kit for the JePPIX InP generic platform at SMART photonics. The design includes a multi-quantum well modulator layer stack consisting of intrinsic InGaAsP wells and barriers with an active layer bandgap of 1.39 μm, the total thickness of the waveguide is 500 nm. The modulator is designed to be compatible with a generic integration platform that allows full monolithic integration of lasers, amplifiers, and passive circuitry. The device cross-section with indications of the key geometric parameters is shown schematically in Figure 1a. Figure 1b shows a microscope image of two of the fabricated devices that includes two input waveguides followed by a 2x2 multi-mode interference (MMI) splitter, a DC phase shifter, a 1 mm or 2 mm CPS phase shifter alongside a wide DC pad used for biasing the modulator, and finally an output 2x2 MMI splitter and 2-output waveguides.

2. Device Characterisation

Determination of $V_\pi L$ was performed by measuring the output optical power, P_{opt}, while sweeping reverse bias voltage. A 1550 nm laser source with an output power of 14 dBm, provided a peak P_{opt} at chip input of 13.5 ± 0.1 dBm. Total fibre-chip losses, for lensed fibres with a 5 μm mode diameter, were estimated to be 9.3 ± 0.5 dB. Input polarisation was optimised by recursively adjusting the polarisation while measuring $P_{opt}(V_{rb})$ to simultaneously maximise the extinction ratio (ER) and minimise V_π. For the 1 and 2 mm devices, values of insertion loss (IL), ER, and V_π are given in Table 1, where IL excludes fibre-chip losses. $V_\pi L$ for the CPS-MZMs is estimated to be 0.7 ± 0.4 Vcm, where the range of $V_\pi L$ arises from the voltage-dependence of V_π from the QCSE [3].

Table 1. Key optical characteristics of a selection of CPS-MZMs. The multiple values of static extinction ratio and half-wave voltage represent the two potential quadrature points (below and above the minimum).

CPS Length (mm)	Insertion loss (dB)	Static extinction ratio (dB)		Half-wave voltage (V)		Used reverse bias voltage (V)	Used extinction ratio (dB)	Estimated −6 dB EE bandwidth (GHz) at V_{rb}
		Q1	Q2	Q1	Q2			
1	8.4 ± 0.5	26.0 ± 0.2	15.3 ± 0.2	9 ± 2	3.4 ± 0.2	10.8	12.6 ± 0.2	~110
2	10.2 ± 0.5	20.0 ± 0.2	11.0 ± 0.2	4.1 ± 0.3	2.9 ± 0.3	8.4	18.4 ± 0.2	~60

Figure 1c provides a schematic of the experimental setup. A 256 GSa/s arbitrary waveform generator (AWG) generated 96-200 GBd OOK, PAM-4, and PAM-8 signals with a peak-peak driving voltage, V_{pp}, of 2.7 V. The signal was digitally pre-emphasised and ran through a raised-cosine pulse-shaping filter with roll-off factor, α, chosen to maximise the signal-to-noise ratio (SNR) at each symbol rate (α = 0.1 above 96 GBd). The signal was terminated using a DC block and 50 Ω load. A stabilised DC voltage was applied to the DC contact pad (Fig. 1b) and thus n-contact layer above the semi-insulating substrate (Fig. 1a), supplying a reverse bias voltage shared across each modulator arm while the RF signal applied is in push-pull configuration. The DC bias voltage was optimised by maximising the SNR of the equalised eye diagram for a 160 GBd PAM-4 signal. The optimal operating V_{rb} was found to be at below the quadrature point, closer to where the optical power variation (in dB) between V_{rb}-(V_{pp}/2) and V_{rb}+(V_{pp}/2) was maximised. This is due to V_{pp} being lower than V_π for both devices and due to the increase in the -6 dB EE bandwidth at higher V_{rb}, from an increasing depletion width [8]. Simulations of the CPS-MZM devices account for the depletion width growth, predicting increased bandwidths at the used V_{rb}. The modulator output is passed through an optical coupler with a split ratio of 1/99, diverting 0.01% to an optical power monitor, while the data signal continues into the receiver comprising an erbium-doped fibre amplifier followed by a tuneable optical filter. Another optical coupler is used to divert 0.1% of the optical power towards an optical spectrum analyser while the rest is passed to an attenuator limiting the average optical power to the photodetector at 8 dBm. Offline digital signal processing DSP was performed where the signal is filtered and resampled to 2 sample/symbol. After that, a T/2-spaced feed-forward equaliser is applied, which has 65 linear term taps and 21 second order term taps.

Figure 2 presents the results of the large signal measurements following digital equalisation. Figure 2a and 2b present the (a) BER and (b) SNR for the full set of applied modulation formats and symbol rates using the CPS-MZM with 1 mm (circle symbols, dashed lines) 2 mm (square symbols, solid lines) electrodes. The 1 mm device shows lower SNR for all symbol rates, despite the larger estimated -6 dB EE bandwidth compared to the 2 mm device. This is due to the 6 dB larger effective ER for the 2 mm device, which itself arises from the lower V_π. Therefore, we centre the following discussion around the 2 mm device. For OOK modulation up to 160 GBd, no bit error is observed. The BER increases for higher symbol rates, reaching the threshold for 25% overhead HD-FEC of 1.82×10^{-2} between 192 GBd and 200 GBd. The measured BER for PAM-4 modulation formats is 1.5×10^{-5} at 96 GBd and remains below the 25% overhead HD-FEC threshold up to 160 GBd (line rate of 320 Gbit/s). PAM-8

modulation formats increase the BER further, but remain below the 25% overhead HD-FEC threshold at 96 GBd (line rate of 288 Gbit/s). The highest measured bit rate for 25% HD-FEC is thus obtained using PAM-4 at 160 GBd. Figure 2c-f provides the eye diagrams of equalised signal using the CPS-MZM with 2 mm long electrodes transmitting (c,d) OOK and (e,f) PAM-4 signals at 128 GBd and 160 GBd, respectively. The eyes for OOK modulation are open while the eyes for PAM-4 modulation become closed but represent the higher achieved bit rates with BER while under the BER thresholds for 6.67% (128 GBd) and 25% (160 GBd) overhead HD-FEC [7].

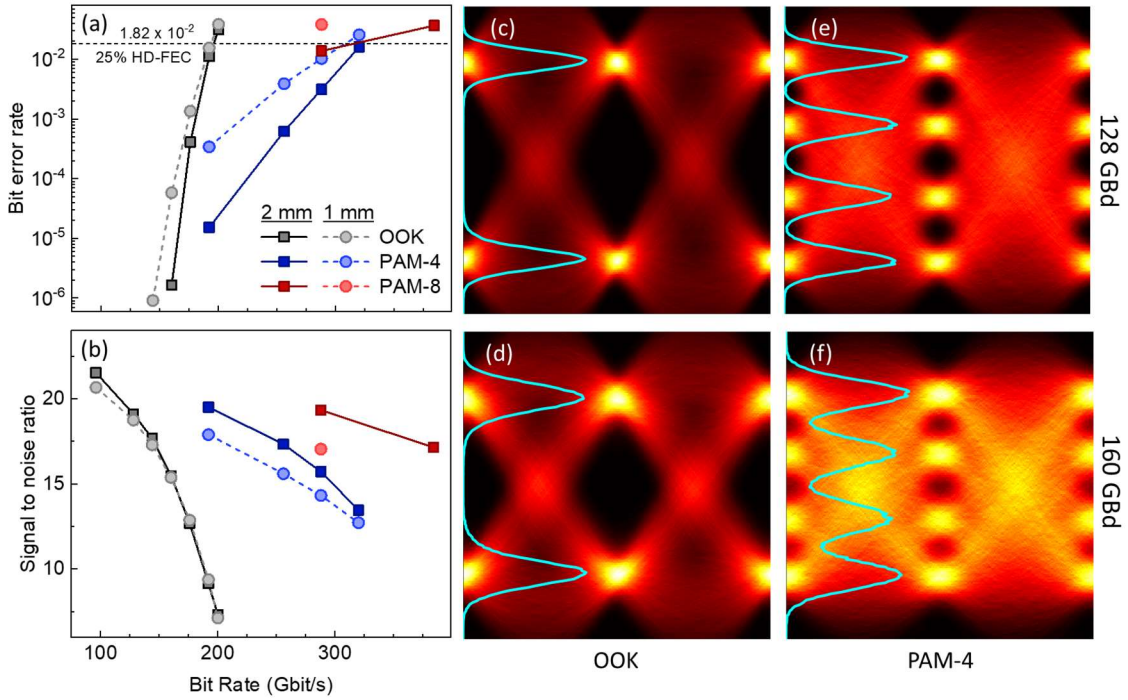

Fig. 2. (a) BER and (b) SNR for the full set of explored modulation formats and symbol rates using the MZM with 2 mm (square symbols, solid lines) and 1 mm (circle symbols, dashed lines) long CPS electrodes. Alongside are the eye diagrams for (c,d) OOK and (e,f) PAM-4 modulation formats at 128 GBd and 160 GBd, respectively. Eye histograms are superimposed onto each eye diagram (cyan lines).

3. Conclusions

We have measured eye diagrams of high-speed CPS-MZM devices fabricated using a generic InP foundry process with specialised layer stacks to allow optimisation of EO efficiency. Further reduction of V_π is possible without compromising the insertion losses of the modulator. We successfully demonstrated PAM-4 transmission up to 160 GBd for the CPS-MZM design with electrode lengths of 2 mm. The devices possess a -6 dB EE bandwidth over V_π figure of merit (FoM) 13 ± 2 GHz/V with an ER of 23 ± 4 dB, where the 2 mm devices show greatest eye opening due to a V_π closer to currently available peak-peak driving voltages at 100 GHz. The CPS-MZM of this work achieved the highest bit rates reported to date for non-coherent InP-based modulators.

3. References

1. G. Sinatkas, T. Christopoulos, O. Tsilipakos, and E. E. Kriezis, "Electro-optic modulation in integrated photonics," J Appl Phys **130**, (2021).
2. Y. Ogiso, Y. Hashizume, H. Tanobe, N. Nunoya, M. Ida, Y. Miyamoto, M. Ishikawa, J. Ozaki, Y. Ueda, H. Wakita, M. Nagatani, H. Yamazaki, M. Nakamura, T. Kobayashi, and S. Kanazawa, "80-GHz Bandwidth and 1.5-V Vπ InP-Based IQ Modulator," Journal of Lightwave Technology **38**, 249–255 (2020).
3. M. Smit, K. Williams, and J. Van Der Tol, "Past, present, and future of InP-based photonic integration," APL Photonics **4**, (2019).
4. A. Meighan, L. Augustin, M. J. Wale, and K. A. Williams, "High-Density 100 GHz-Class Mach-Zehnder Modulators integrated in a InP Generic Foundry Platform," in *2022 Conference on Lasers and Electro-Optics (CLEO)* (2022), pp. 1–3.
5. L. M. Augustin, R. Santos, E. den Haan, S. Kleijn, P. J. A. Thijs, S. Latkowski, D. Zhao, W. Yao, J. Bolk, H. Ambrosius, S. Mingaleev, A. Richter, A. Bakker, and T. Korthorst, "InP-Based Generic Foundry Platform for Photonic Integrated Circuits," IEEE Journal of Selected Topics in Quantum Electronics **24**, 1–10 (2018).
6. J. A. Hillier, A. Meighan, M. Van Den Hout, S. Van Der Heide, S. Cakmakyapan, W. Yao, R. Van Dommele, M. Wale, C. Okonkwo, and K. Williams, "A 100 GBaud co-planar stripline Mach-Zehnder modulator on Indium Phosphide platform," in *2023 Opto-Electronics and Communications Conference, OECC 2023* (Institute of Electrical and Electronics Engineers Inc., 2023).
7. L. M. Zhang and F. R. Kschischang, "Staircase codes with 6% to 33% overhead," Journal of Lightwave Technology **32**, 1999–2002 (2014).
8. W. Shockley, "The Theory of *p-n* Junctions in Semiconductors and *p-n* Junction Transistors," Bell System Technical Journal **28**, 435–489 (1949).